Histone H2AX stabilizes broken DNA strands to suppress chromosome breaks and translocations during V(D)J recombination

Bu Yin,[1,2,4] Velibor Savic,[1,2,4] Marisa M. Juntilla,[2,3] Andrea L. Bredemeyer,[5] Katherine S. Yang-Iott,[2,4] Beth A. Helmink,[5] Gary A. Koretzky,[2,3] Barry P. Sleckman,[5] and Craig H. Bassing[1,2,4]

[1]Cell and Molecular Biology Graduate Group, [2]Abramson Family Cancer Research Institute, and [3]Department of Medicine, University of Pennsylvania School of Medicine, Philadelphia, PA 19104
[4]Department of Pathology and Laboratory Medicine, Center for Childhood Cancer Research, Children's Hospital of Philadelphia, Philadelphia, PA 19104
[5]Department of Pathology and Immunology, Washington University School of Medicine, St Louis, MO 63110

The H2AX core histone variant is phosphorylated in chromatin around DNA double strand breaks (DSBs) and functions through unknown mechanisms to suppress antigen receptor locus translocations during V(D)J recombination. Formation of chromosomal coding joins and suppression of translocations involves the ataxia telangiectasia mutated and DNA-dependent protein kinase catalytic subunit serine/threonine kinases, each of which phosphorylates H2AX along cleaved antigen receptor loci. Using Abelson transformed pre–B cell lines, we find that H2AX is not required for coding join formation within chromosomal V(D)J recombination substrates. Yet we show that H2AX is phosphorylated along cleaved Igκ DNA strands and prevents their separation in G1 phase cells and their progression into chromosome breaks and translocations after cellular proliferation. We also show that H2AX prevents chromosome breaks emanating from unrepaired RAG endonuclease-generated TCR-α/δ locus coding ends in primary thymocytes. Our data indicate that histone H2AX suppresses translocations during V(D)J recombination by creating chromatin modifications that stabilize disrupted antigen receptor locus DNA strands to prevent their irreversible dissociation. We propose that such H2AX-dependent mechanisms could function at additional chromosomal locations to facilitate the joining of DNA ends generated by other types of DSBs.

CORRESPONDENCE
Craig H. Bassing:
bassing@email.chop.edu

Abbreviations used: 2D-2C-FISH, two-dimensional two-color DNA FISH; ATM, ataxia telangiectasia mutated; ChIP, chromatin immunoprecipitation; CSR, class switch recombination; DNA-PKcs, DNA-dependent protein kinase catalytic subunit; DSB, double strand break; FISH, fluorescent in situ hybridization; MRN, Mre11–Rad50–Nbs1; NHEJ, nonhomologous end joining.

The rapid phosphorylation of histone H2A proteins in chromatin for large distances around DNA double strand breaks (DSBs) is a conserved feature of the cellular DNA damage response. In mammalian cells, the H2AX histone variant comprises 2–25% of the H2A pool and is non-uniformly incorporated into chromatin (Rogakou et al., 1998; Bewersdorf et al., 2006). Upon DSB induction, the ataxia telangiectasia mutated (ATM), DNA-dependent protein kinase catalytic subunit (DNA-PKcs), and ATR (ATM and Rad3 related) protein kinases phosphorylate H2AX on a conserved carboxyl terminal serine residue to form γ-H2AX around DNA breakage sites (Rogakou et al., 1999; Paull et al., 2000; Burma et al., 2001; Ward and Chen, 2001; Stiff et al., 2004). Generation of γ-H2AX creates binding sites for repair and checkpoint proteins, some of which catalyze other covalent modifications of γ-H2AX to generate binding sites for additional repair and checkpoint proteins, all of which assemble into complexes in chromatin surrounding DNA breaks (Downs et al., 2007; Bonner et al., 2008). *H2ax*$^{-/-}$ cells exhibit increased sensitivity to agents that cause DSBs, elevated levels of spontaneous and DSB-induced genomic instability, and defective repair of chromosomal DSBs (Bassing et al., 2002a; Celeste et al., 2002; Xie et al., 2004; Franco et al., 2006). Although *H2ax*$^{-/-}$ cells display apparent normal activation of p53-dependent cell cycle checkpoints and apoptotic responses (Bassing

The Rockefeller University Press $30.00
J. Exp. Med. Vol. 206 No. 12 2625-2639
www.jem.org/cgi/doi/10.1084/jem.20091320

et al., 2002a; Celeste et al., 2002), *H2ax*$^{-/-}$ cells are defective in the G2/M checkpoint after induction of only a few DSBs (Fernandez-Capetillo et al., 2002). The phenotypes of *H2ax*$^{-/-}$ cells suggest that the ability of γ-H2AX to retain repair and checkpoint proteins around DSBs may promote accessibility of DNA ends, stabilize disrupted DNA strands, and/or amplify checkpoint signals (Bassing and Alt, 2004; Stucki and Jackson, 2006; Bonner et al., 2008; Kinner et al., 2008).

The health and survival of humans and mice depends on the ability of their adaptive immune systems to generate lymphocytes with receptors capable of recognizing and eliminating large varieties of pathogens. In developing lymphocytes, Ig and TCR variable region exons are assembled from germline V (variable), D (diversity), and J (joining) gene segments by the lymphoid-specific RAG1/RAG2 (RAG) endonuclease and the ubiquitously expressed nonhomologous end-joining (NHEJ) DSB repair factors (Bassing et al., 2002b). The RAG proteins catalyze the coupled cleavage of DNA strands between a pair of gene segments and their flanking recombination signal sequences to generate covalently sealed coding ends (CEs) and blunt signal ends (SEs; Fugmann et al., 2000). RAG-mediated cleavage occurs only in G1 phase because of cell cycle phase-restricted expression of RAG2 (Lee and Desiderio, 1999). The DNA-PKcs/Artemis endonuclease opens CEs (Ma et al., 2002), which are then processed by nucleases and polymerases (McElhinny and Ramsden, 2004). Core NHEJ factors join together CEs and SEs to form coding joins (CJs) and signal joins (SJs), respectively (Bassing et al., 2002b). RAG1/RAG2 can hold CEs and SEs within stable synaptic complexes (Agrawal and Schatz, 1997; Lee et al., 2004); however, ATM and, likely, the Mre11–Rad50–Nbs1 (MRN) complex maintain chromosomal CEs in proximity to facilitate end-joining in G1 phase cells (Bredemeyer et al., 2006; Deriano et al., 2009; Helmink et al., 2009). The large combination of V(D)J joining events and the imprecision in CJ formation cooperate to generate a diverse repertoire of antigen receptor specificities.

Despite its benefits, V(D)J recombination poses substantial threats to the viability and genomic integrity of lymphocytes and lymphoma predisposition in host organisms. For example, DNA-PKcs–deficient mice lack mature lymphocytes as a result of inability to repair RAG-generated DSBs, but they only occasionally develop lymphoma (Bosma et al., 1983; Gao et al., 1998; Taccioli et al. 1998). However, DNA-PKcs/p53–deficient mice rapidly succumb to pro-B lymphomas with RAG-dependent IgH/c-myc translocations (Vanasse et al., 1999; Gladdy et al., 2003), demonstrating that p53 protects organisms from oncogenic translocations during V(D)J recombination. RAG-generated DSBs activate ATM (Perkins et al., 2002; Bredemeyer et al., 2008), which is required for both normal coding join formation and normal p53 activation (Perkins et al., 2002; Bredemeyer et al., 2006). Consequently, *Atm*$^{-/-}$ mice exhibit impaired lymphocyte development, increased frequencies of antigen receptor locus translocations in nonmalignant lymphocytes, and marked predisposition to thymic lymphomas with RAG-dependent TCR-α/δ translocations (Barlow et al., 1996; Elson et al., 1996; Xu et al., 1996; Borghesani et al., 2000; Liyanage et al., 2000; Petiniot et al., 2000, 2002; Callén et al., 2007; Matei et al., 2007; Vacchio et al., 2007). The observation that RAG-dependent γ-H2AX foci colocalized with TCR-α/δ loci suggested that H2AX may coordinate DSB repair, signaling, and surveillance during V(D)J recombination (Chen et al., 2000). Consistent with this notion, αβ T cells of *H2ax*$^{-/-}$ mice contain elevated frequencies of TCR-α/δ translocations and *H2ax*$^{-/-}$*p53*$^{-/-}$ mice develop pro–B lymphomas with RAG-dependent IgH/c-myc translocations (Celeste et al., 2002, 2003; Bassing et al., 2003, 2008). ATM and DNA-PKcs generate γ-H2AX along RAG-cleaved DNA strands (Savic et al., 2009). However, *H2ax*$^{-/-}$ mice do not exhibit impaired or blocked lymphocyte development, as observed in mice deficient for ATM or DNA-PKcs, suggesting that H2AX is not involved in the processing and/or joining of chromosomal coding ends. However, H2AX prevents the progression of IgH locus DNA breaks into chromosome breaks and translocations during class switch recombination (CSR; Franco et al., 2006; Ramiro et al., 2006), which is consistent with the notion that H2AX does function in chromosomal end joining (Reina-San-Martin et al., 2003; Bassing and Alt, 2004). Consequently, the mechanisms by which H2AX suppresses antigen receptor locus translocations during V(D)J recombination remain unknown.

Based on the disparate phenotypes of *Atm*$^{-/-}$ and *H2ax*$^{-/-}$ mice, we hypothesized that formation of γ-H2AX for long distances along RAG-cleaved antigen receptor loci promotes chromatin changes that hold together broken DNA strands (Bassing and Alt, 2004). We proposed that this stabilization of disrupted DNA strands would not be required for coding join formation in the G1 phase of developing lymphocytes but that this H2AX-dependent function would be important for preventing the irreversible dissociation of unrepaired coding ends persisting into S phase (Bassing and Alt, 2004). Quantitative analysis of DNA end joining during V(D)J recombination of endogenous loci in developing lymphocytes is difficult because of asynchronous induction of RAG DSBs at multiple genomic locations in cycling cells and expansion of lymphocytes in which functional coding joins have been assembled. Consequently, we have used a cell line–based system that enables the controlled induction of RAG DSBs at single defined chromosomal locations in G1-arrested cells to test our hypothesized functions of H2AX during V(D)J recombination.

RESULTS

H2AX-deficient cells exhibit normal coding join formation within chromosomal substrates

Although H2AX is not required for coding join formation in extrachromosomal substrates (Bassing et al., 2002a), the phosphorylation of H2AX could function downstream of ATM to facilitate chromosomal coding join formation. To investigate potential H2AX function in chromosomal end joining during V(D)J recombination, we generated multiple independently derived immortalized abl pre–B cell lines from two different *H2ax*$^{F/F}$ mice containing floxed *H2ax* loci on both alleles.

H2ax$^{F/F}$ cells express normal amounts of H2AX and exhibit phenotypes indistinguishable from those of wild-type cells (Bassing et al., 2002a). Treatment of abl pre–B cells with STI571, an inhibitor of the abl kinase, causes G1 arrest, induction of RAG expression, and robust rearrangement of endogenous Igκ loci and V(D)J recombination substrates (Muljo and Schlissel, 2003; Bredemeyer et al., 2006). V(D)J recombination of the chromosomally integrated pMX-DEL^{CJ} retroviral substrate results in formation of a coding join within the chromosome and generation of a signal join on an extrachromosomal circle (Fig. 1 a). We transduced *H2ax*$^{F/F}$ abl pre–B cell lines with the pMX-DEL^{CJ} retroviral recombination substrate and used limiting dilution to isolate independent *H2ax*$^{F/F}$ clones with single pMX-DEL^{CJ} substrates integrated into their genome (*H2ax*$^{F/F}$*:DEL*^{CJ} cells). We next incubated individual *H2ax*$^{F/F}$*:DEL*^{CJ} lines with TAT-Cre protein to delete the floxed *H2ax* alleles and again used limiting dilution to recover *H2ax*$^{F/F}$*:DEL*^{CJ} and *H2ax*$^{\Delta/\Delta}$*:DEL*^{CJ} clones with pMX-DEL^{CJ} substrates integrated at identical genomic locations. The genotypes of these clones were confirmed by both PCR and Southern blot analyses that distinguish between the *H2ax*^{F} and *H2ax*$^{\Delta}$ alleles (unpublished data).

To evaluate potential H2AX function in chromosomal end-joining during V(D)J recombination, we sought to monitor the repair of RAG-generated CEs within identical pMX-DEL^{CJ} integrants in two different *H2ax*$^{F/F}$*:DEL*^{CJ} and *H2ax*$^{\Delta/\Delta}$*:DEL*^{CJ} clones of the same passage. The induction and repair of RAG-generated DSBs within integrated pMX-DEL^{CJ} substrates can be monitored by Southern blot analysis that distinguishes between uncleaved (GL) substrates, cleaved but not repaired (CE) substrates, and cleaved and repaired (CJ) substrates (Fig. 1 a). Thus, we conducted Southern blotting of identical pMX-DEL^{CJ} integrants in two *H2ax*$^{F/F}$*:DEL*^{CJ} and *H2ax*$^{\Delta/\Delta}$*:DEL*^{CJ} clones treated with STI571 for increasing amounts of time. As a control for the accumulation of unrepaired chromosomal CEs, we also conducted Southern blot analysis of *Artemis*$^{-/-}$*:DEL*^{CJ} clones. After 48 h of STI571 treatment, we observed loss of the pMX-DEL^{CJ} GL fragment and appearance of the pMX-DEL^{CJ} CJ fragment to similar extents in the two *H2ax*$^{F/F}$*:DEL*^{CJ} and *H2ax*$^{\Delta/\Delta}$*:DEL*^{CJ} clones assayed (Fig. 1 b). In contrast, we detected loss of the pMX-DEL^{CJ} GL fragment and appearance of the pMX-DEL^{CJ} CE fragment at 24 h of STI571 treatment in *Artemis*$^{-/-}$*:DEL*^{CJ} cells (Fig. 1 b). At each time point assayed between 48 and 96 h of STI571 treatment, we observed similar increasing loss of the pMX-DEL^{CJ} GL fragment and appearance of the pMX-DEL^{CJ} CJ fragment in *H2ax*$^{F/F}$*:DEL*^{CJ} and *H2ax*$^{\Delta/\Delta}$*:DEL*^{CJ} cells (Fig. 1 b) but increasing loss of the pMX-DEL^{CJ} GL fragment and appearance of the pMX-DEL^{CJ} CE fragment in *Artemis*$^{-/-}$*:DEL*^{CJ} cells (Fig. 1 b). Notably, despite conducting Southern analysis on twice as much genomic DNA for *H2ax*$^{F/F}$*:DEL*^{CJ} and *H2ax*$^{\Delta/\Delta}$*:DEL*^{CJ} cells than for *Artemis*$^{-/-}$*:DEL*^{CJ} cells, we were unable to detect the pMX-DEL^{CJ} CE fragment in *H2ax*$^{\Delta/\Delta}$*:DEL*^{CJ} cells. These data demonstrate that, unlike deficiency in ATM or DNA-PKcs (Bredemeyer et al., 2006), H2AX deficiency does not lead to an observable accumulation of unrepaired coding ends during V(D)J recombination of chromosomal substrates within G1-phase cells.

Because lymphomas with RAG-dependent antigen receptor locus translocations arise at a higher frequency in *H2ax*$^{-/-}$ *p53*$^{-/-}$ mice than in *H2ax*$^{-/-}$ mice (Bassing et al., 2003; Celeste et al., 2003), we considered the possibility that p53 deficiency might reveal a role of H2AX in formation of chromosomal coding joins in G1-phase cells. To investigate this issue, we generated two independently derived abl pre–B cell lines from different *H2ax*$^{F/F}$ mice also containing floxed *p53* exons on both alleles. We used TAT-Cre to generate *H2ax*$^{F/F}$*p53*$^{F/F}$*:DEL*^{CJ} and *H2ax*$^{\Delta/\Delta}$*p53*$^{\Delta/\Delta}$*:DEL*^{CJ} clones of the same passage with pMX-DEL^{CJ} substrates integrated at identical genomic locations. Southern blot analysis of identical pMX-DEL^{CJ} integrants in two different *H2ax*$^{F/F}$*p53*$^{F/F}$*:DEL*^{CJ} and *H2ax*$^{\Delta/\Delta}$*p53*$^{\Delta/\Delta}$*:DEL*^{CJ} clones treated with STI571 for increasing amounts of time revealed similar increasing loss of the pMX-DEL^{CJ} GL fragment and appearance of the pMX-DEL^{CJ} CJ fragment in the two *H2ax*$^{F/F}$*p53*$^{F/F}$*:DEL*^{CJ} and *H2ax*$^{\Delta/\Delta}$*p53*$^{\Delta/\Delta}$*:DEL*^{CJ} cells (Fig. 1 c). Again, despite conducting Southern analysis on twice as much genomic DNA for *H2ax*$^{F/F}$*p53*$^{F/F}$*:DEL*^{CJ} and *H2ax*$^{\Delta/\Delta}$ *p53*$^{\Delta/\Delta}$*:DEL*^{CJ} cells as for *Artemis*$^{-/-}$*:DEL*^{CJ} cells, we did not observe detectable levels of the pMX-DEL^{CJ} CE fragment in *H2ax*$^{\Delta/\Delta}$*p53*$^{\Delta/\Delta}$*:DEL*^{CJ} cells (Fig. 1 c). These data further support the notion that H2AX is not required for end joining of chromosomal coding ends in G1-phase lymphocytes.

Because RAG-dependent formation of γ-H2AX occurs at Jκ segments and over adjacent sequences extending away from the Igκ locus (Savic et al., 2009), we also considered that H2AX might be required for resolution of Jκ CEs. The mouse Igκ locus resides on chromosome 6 and is composed of 140 Vκs spanning 2 Mb and four functional Jκs spanning 1.8 kb and residing 60 kb from the Vκs. Igκ locus V(D)J recombination occurs through the coupled cleavage and subsequent joining of a Vκ and Jκ segment. Because of the small size of the Jκ cluster, Southern blot analysis with a 3′ Jκ probe can be used to monitor and quantify the induction of RAG-generated Igκ locus DSBs (Fig. 2 a). Thus, we next conducted Southern blotting of *H2ax*$^{-/-}$ pre–B cells either untreated or treated with STI571 for 72 h. As a control for the accumulation of unrepaired Jκ CEs, we also conducted Southern blot analysis of previously described *Artemis*$^{-/-}$ cells (Helmink et al., 2009). We observed decreased intensity of the Jκ GL band in both *H2ax*$^{-/-}$ and *Artemis*$^{-/-}$ cells treated with STI571, and appearance of bands corresponding to Jκ CEs in STI571-treated *Artemis*$^{-/-}$ cells but not in STI571-treated *H2ax*$^{-/-}$ cells (Fig. 2 a). These data indicate that H2AX deficiency does not result in the detectable accumulation of unrepaired Igκ coding ends in G1-phase cells. Consequently, we conclude that H2AX function is not required for chromosomal end joining during V(D)J recombination in G1-phase lymphocytes.

H2AX-dependent chromatin changes prevent separation of RAG-cleaved Igκ DNA strands in G1-phase cells

We first sought to define the entire γ-H2AX chromatin domain formed along Igκ loci during V(D)J recombination in G1-phase cells. For this purpose, we conducted chromatin

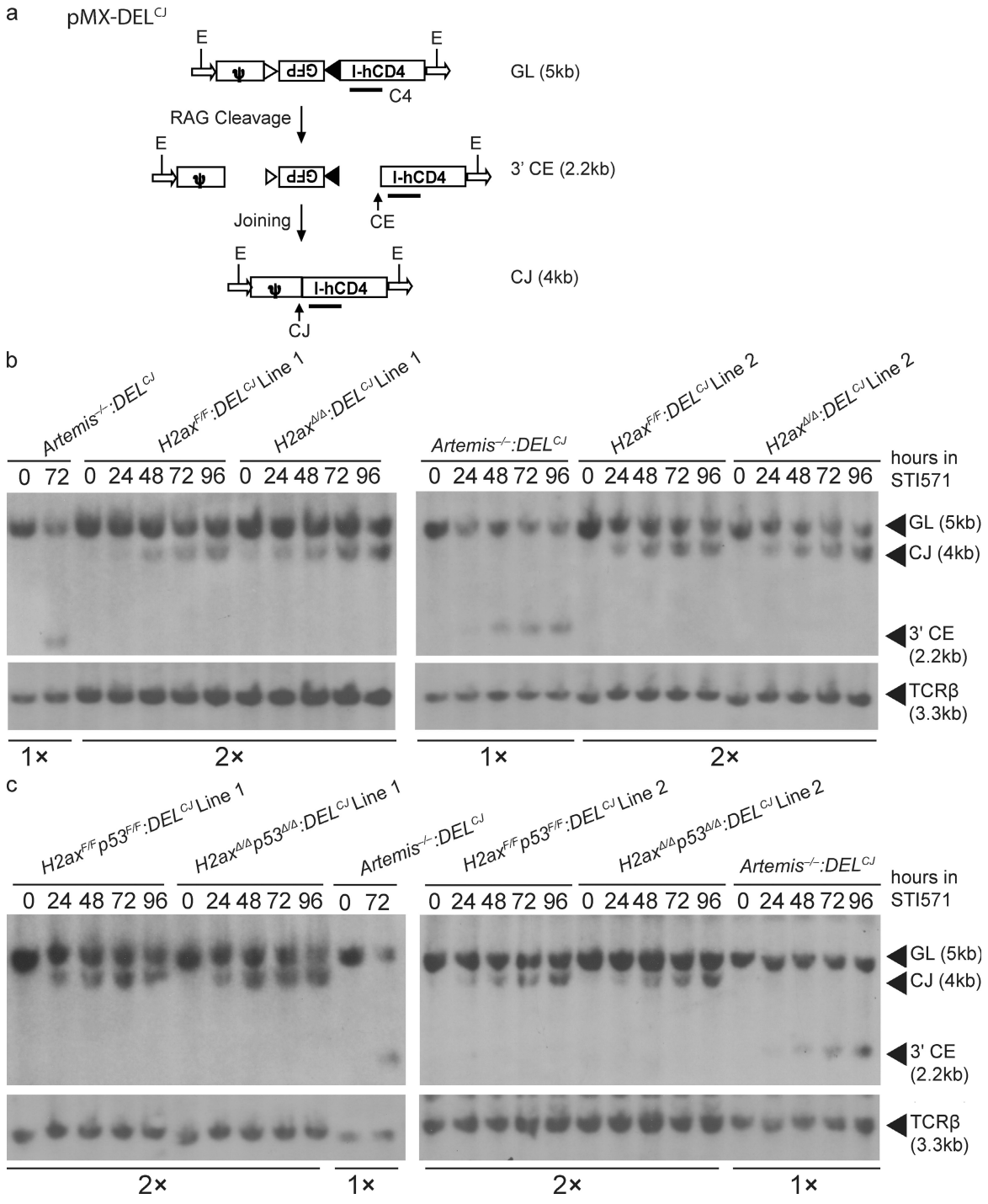

Figure 1. H2AX-deficient cells exhibit normal coding join formation within chromosomal substrates. (a) Shown are schematic diagrams of the pMX-DEL^{CJ} V(D)J recombination substrate in the uncleaved (GL), cleaved but not repaired (CE), and cleaved and repaired (CJ) configurations. The recombination signal sequences are represented by triangles. Arrows represent the LTR sequences. Indicated are the relative positions of the EcoRV sites (E) and C4 probe used for Southern blot analysis and the sizes of the C4-hybridizing EcoRV fragments in pMX-DEL^{CJ} substrates of the GL, CE, and CJ configuration. (b and c) Southern blot analysis of recombination products generated in cells of two different *H2ax$^{F/F}$:DEL^{CJ}* and *H2ax$^{\Delta/\Delta}$:DEL^{CJ}* abl pre–B cell lines (b) or *H2ax$^{F/F}$p53$^{F/F}$:DEL^{CJ}* and *H2ax$^{\Delta/\Delta}$p53$^{\Delta/\Delta}$:DEL^{CJ}* abl pre–B cell lines (c) treated with STI571 for the indicated times. EcoRV-digested genomic DNA was hybridized with the C4 probe. The bands corresponding to pMX-DEL^{CJ} substrates of the GL, CE, and CJ configurations are indicated. Blots were stripped and then probed with a TCR-β probe as a control for DNA content. *Artemis$^{-/-}$:DEL^{CJ}* abl pre–B cell lines were used as a positive control for detection of pMX-DEL^{CJ} CEs, with half as much genomic DNA loaded to increase the sensitivity of detection for pMX-DEL^{CJ} CEs in experimental cells. These data are representative of experiments performed more than three independent times.

immunoprecipitation (ChIP) to measure γ-H2AX densities in nucleosomes on DNA strands located within and adjacent to Igκ loci in *Artemis*$^{-/-}$ pre–B cells, either untreated or treated with STI571 for 96 h to ensure complete RAG-mediated cleavage. We used *Artemis*$^{-/-}$ cells rather than wild-type cells because the accumulation of unrepaired coding ends enhances ability to detect γ-H2AX along RAG-cleaved antigen receptor loci (Savic et al., 2009). Using ChIP, we detected significant increases in γ-H2AX densities within Igκ and for ∼500 kb on both sides of Igκ in STI571-treated *Artemis*$^{-/-}$

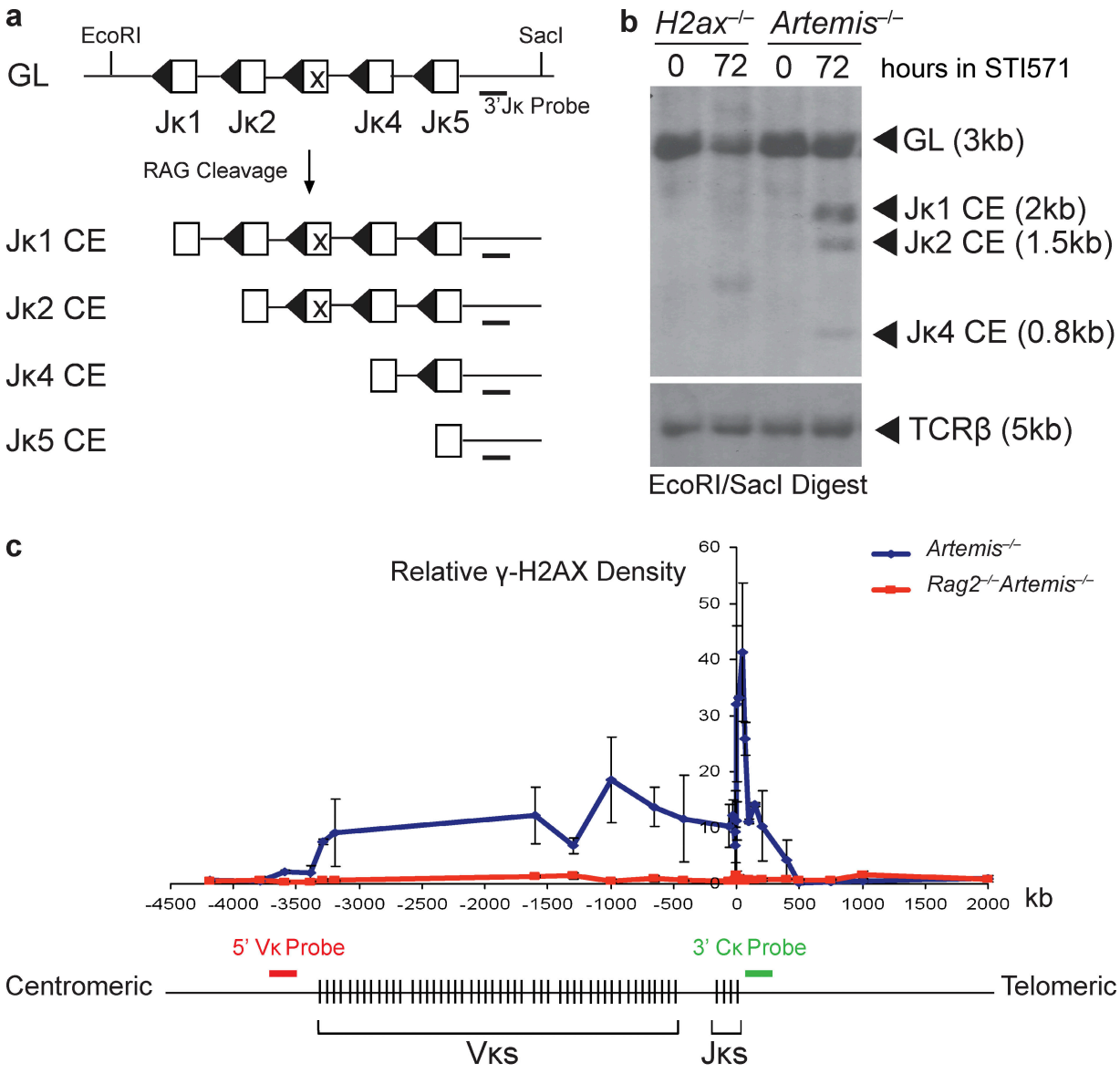

Figure 2. No accumulation of Jκ coding ends in the absence of H2AX phosphorylation along RAG-cleaved Igκ DNA strands. (a) Shown are schematic diagrams of the Jκ cluster of the Igκ locus in the uncleaved (GL) and cleaved but not repaired (CE) configurations. Open boxes represent the Jκ segments and triangles their recombination signal sequences. Indicated are the relative positions of the EcoRI and SacI sites and 3′Jκ probe used for Southern blot analysis. (b) Southern blot analysis of recombination products generated in *H2ax*$^{-/-}$ and *Artemis*$^{-/-}$ abl pre–B cell lines, either untreated or treated with STI571 for 72 h. EcoRI–SacI-digested genomic DNA was hybridized with the 3′Jκ probe. The bands corresponding to Jκ loci of the GL and CE configurations are indicated. The STI571-treated *H2ax*$^{-/-}$ cells harbor a band that likely represents a predominant VκJκ rearrangement. Blots were stripped and then probed with a TCR-β probe as a control for DNA content. These data are representative of experiments performed >10 independent times. (c) Schematic diagram of the mouse Igκ locus and graphical representation of γ-H2AX densities as determined by ChIP at locations along DNA strands within and adjacent to Igκ in *Artemis*$^{-/-}$ abl pre–B cells treated with STI571 for 96 h. The 0-kb value of the x-axis corresponds to the 3′ end of the Jκ5 coding segment. The negative and positive values represent the distances centromeric and telomeric, respectively, from the 3′ end of Jκ5. Red and green bars indicate the approximate genomic locations to which the 5′ Vκ (RP24-243E11) and 3′ Cκ (RP23-341D5) BACs hybridize. The lengths of these bars are not drawn to scale. These data are representative of experiments performed >20 independent times. Error bars indicate standard deviation of three independent experiments.

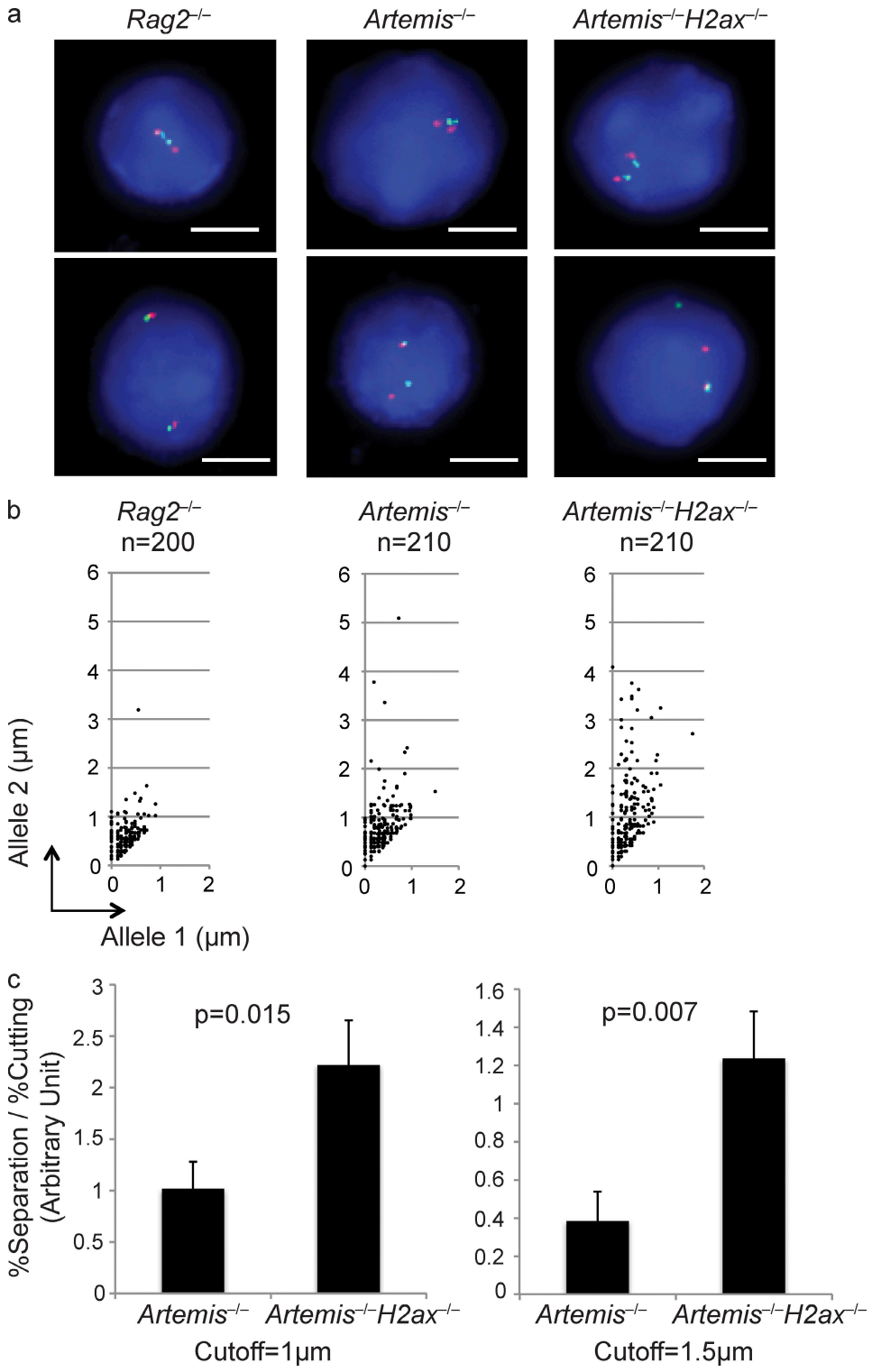

Figure 3. H2AX suppresses separation of RAG-cleaved Igκ locus DNA strands. (a) Shown are representative fluorescent light microscopy images of 2C-FISH analysis conducted on G1-phase nuclei of *Rag2*$^{-/-}$, *Artemis*$^{-/-}$, and *Artemis*$^{-/-}$*H2ax*$^{-/-}$ abl pre-B cells treated with STI571 for 96 h. Nuclei were hybridized with the 5′ Vκ (red) and 3′ Cκ (green) BACs and stained with DAPI to visualize DNA. The representative *Rag2*$^{-/-}$ image shows a nucleus with coincident probe hybridization signals on both Igκ alleles. The top nucleus contains paired Igκ alleles and the bottom unpaired Igκ alleles. The representative *Artemis*$^{-/-}$ and *Artemis*$^{-/-}$*H2ax*$^{-/-}$ images each shows nuclei with coincident probe signals on both Igκ alleles and paired Igκ alleles (top) or noncoincident probe signals on one Igκ allele, overlapping probe hybridization on the other Igκ allele, and unpaired Igκ alleles (bottom). Bars, ∼3 μm. (b) Shown are representative scatter plots depicting the distances between red and green signals on allele 1 (shorter distance) and allele 2 (longer

pre–B cells (Fig. 2 c). The γ-H2AX densities formed telomeric of the Jκ segments were greater than those formed over the Vκ cluster (Fig. 2 c). The numbers of Vκ and Jκ DSBs within our experimental population of cells must be equal because V(D)J recombination proceeds through coupled cleavage. Because the Igκ locus contains a cluster of 140 Vκ segments spanning 2 Mb and a cluster of four functional Jκ segments spanning 1.8 kb, the chromosomal density of Vκ cluster DSBs should be less than the chromosomal density of Jκ cluster DSBs within our experimental population of cells. Thus, the simplest explanation for the observed γ-H2AX pattern across the Igκ locus is that it reflects the density of DSBs induced at the assayed genomic locations. However, these observations are also consistent with the notion that different features of local chromatin environment among the Vκ segments and downstream of the Jκ segments may influence γ-H2AX dynamics. Regardless, our data demonstrate that a γ-H2AX chromatin domain forms along chromosomal DNA strands containing RAG-cleaved Igκ loci for distances extending at least 500 kb from Igκ coding ends.

To test our hypothesis that H2AX-mediated chromatin changes function to hold together broken DNA strands, we sought to monitor the positional stability of RAG-cleaved Igκ loci in G1-phase cells. We have previously used two-dimensional two-color DNA fluorescent in situ hybridization (FISH [2D-2C-FISH]) with a 5′ Vκ BAC (RP24-243E11) and a 3′ Cκ BAC (RP23-341D5) probe to monitor the positional stability of RAG-cleaved Igκ locus DNA strands in STI571-treated *Artemis*$^{-/-}$*p53*$^{-/-}$ and *Artemis*$^{-/-}$*Atm*$^{-/-}$ abl pre–B cells (Hewitt et al., 2009). These 5′ Vκ and 3′ Cκ probes hybridize to genomic sequences located near the ends of γ-H2AX domain that forms along RAG-cleaved Igκ loci within STI571 treated pre–B cells (Fig. 2 c). 2D-FISH cannot distinguish between signals that appear on top of each other that are really separate and, therefore, likely underestimates the numbers of cells with unstabilized Igκ locus DNA ends. However, because this should be equal across cells of different genotypes, conclusions about different genotypes relative to each other are still possible with 2D-2C-FISH.

We first conducted 2D-2C-FISH using these 5′ Vκ and 3′ Cκ probes on G1 interphase nuclei prepared from three independent *Rag2*$^{-/-}$ abl pre–B cells treated with STI571 for 96 h (Fig. 3 a). We measured the distances between 5′ Vκ (red) and 3′ Cκ (green) signals on both alleles in ∼200 nuclei of each cell line assayed, designated the shorter distance from allele 1 and the longer distance from allele 2, and plotted these values onto scatter plots. We observed overlapping or coincident probe hybridization signals (<1 μm apart) on both alleles in >95% of nuclei and noncoincident signals on one allele in <4% of nuclei (Fig. 3 b). Using three independent *Artemis*$^{-/-}$ cell lines, we observed overlapping or coincident probe signals on both alleles in ∼80% of nuclei and noncoincident probe signals on a single allele in ∼20% of nuclei (Fig. 3 b). With three independent *Artemis*$^{-/-}$*H2ax*$^{-/-}$ cell lines, we observed overlapping or coincident probe signals on both alleles in ∼60% of nuclei and noncoincident probe signals on a single allele in ∼40% of nuclei (Fig. 3 b). Although similar levels of unrepaired Igκ locus CEs accumulated in all *Artemis*$^{-/-}$ and *Artemis*$^{-/-}$ *H2ax*$^{-/-}$ cells assayed (not depicted), we also normalized the percentage of nuclei with noncoincident probe hybridization signals to the extent of Igκ locus cleavage (Fig. 3 c). These data show that RAG-cleaved Igκ locus DNA strands physically separate in a significantly higher percentage of *Artemis*$^{-/-}$ *H2ax*$^{-/-}$ cells than in *Artemis*$^{-/-}$ cells. Similar results were obtained using a larger distance (>1.5 μm) to score noncoincident hybridization (Fig. 3 c). Consequently, we conclude that γ-H2AX–mediated chromatin changes suppress physical separation of RAG-cleaved antigen receptor loci in G1-phase cells to prevent their irreversible disassociation or aberrant joining.

H2AX prevents transition of RAG-cleaved DNA strands into chromosome breaks and translocations during cellular proliferation

Molecular characterization of IgH/c-myc translocations in *H2ax*$^{-/-}$*p53*$^{-/-}$ pro–B lymphomas revealed that these lesions occurred after the replication of chromosomes containing unrepaired RAG-initiated IgH locus DNA breaks (Bassing et al., 2003; Celeste et al., 2003). Thus, we hypothesized that γ-H2AX formation along RAG-cleaved antigen receptor loci promotes chromatin changes that hold together broken DNA strands to prevent unrepaired coding ends from transitioning into chromosome breaks and translocations during S phase (Bassing and Alt, 2004). To test our hypothesis, we sought to quantify the frequency of Igκ chromosome breaks and translocations in *H2ax*$^{-/-}$, *Artemis*$^{-/-}$, and *Artemis*$^{-/-}$*H2ax*$^{-/-}$ abl pre–B cell lines treated with STI571 and then released back into cell cycle by STI571 removal. For this purpose, we hybridized chromosome 6–specific paints (red) and conducted FISH with the 5′ Vκ and 3′ Cκ BACs (green) on 100 or more metaphase spreads prepared from untreated cells or cells that had been treated with STI571 and then released back into cell cycle (Fig. 4 a). We found chromosome 6 chromosome breaks

distance) in G1-phase nuclei of *Rag2*$^{-/-}$, *Artemis*$^{-/-}$, and *Artemis*$^{-/-}$*H2ax*$^{-/-}$ abl pre–B cells treated with STI571 for 96 h. The numbers of nuclei assayed to generate the representative data are indicated. These data are representative of experiments performed three independent times. (c) Shown are bar graphs depicting in arbitrary units the nuclei with separated RAG-cleaved Igκ DNA strands normalized to the extent of cutting in three experiments conducted on cells of independent *Artemis*$^{-/-}$ and *Artemis*$^{-/-}$*H2ax*$^{-/-}$ abl pre–B cells treated with STI571 for 96 h. To obtain these data, the percentage of nuclei with separated signals was divided by the percentage of RAG-cleaved Igκ alleles within the population of treated cells. The graphs use either 1 μm (left) or 1.5 μm (right) as the cutoff for distinction between coincident or overlapping versus noncoincident probe hybridization signals. The p-values for comparison between cells of different genotypes are indicated. These data were obtained from the same experiment performed three independent times. Error bars indicate standard deviation of three independent experiments.

or translocations in <1% of metaphases prepared from untreated *H2ax*$^{-/-}$, *Artemis*$^{-/-}$, or *Artemis*$^{-/-}$*H2ax*$^{-/-}$ cells of three different cell lines for each genotype (Fig. 4, a and b). These data indicate that structural abnormalities of chromosome 6 are not frequent occurrences in abl pre–B cells with deficiencies in H2AX and/or Artemis. We also detected chromosome 6 abnormalities in <1% of metaphases prepared from *H2ax*$^{-/-}$ or *Artemis*$^{-/-}$ cells treated and then released from STI571 (Fig. 4, a and b). However, we observed chromosome 6 breaks or translocations involving Igκ in 4–5% of metaphases prepared from *Artemis*$^{-/-}$*H2ax*$^{-/-}$ cells treated and then released from STI571 (Fig. 4, a and b). Southern blot analysis of STI571-treated cells before removal of the STI571 revealed similar levels of unrepaired Igκ locus DSBs in all cells (unpublished data). These data suggest that unrepaired Igκ locus coding ends progress into chromosome breaks and translocations at a significantly higher frequency in *Artemis*$^{-/-}$*H2ax*$^{-/-}$ cells than in *Artemis*$^{-/-}$ or *H2ax*$^{-/-}$ cells after STI571 treatment and release. We also found chromosome 6 breaks and translocations involving Igκ in a significantly higher percentage of ST1571-treated and released *H2ax*$^{-/-}$*Artemis*$^{-/-}$*p53*$^{-/-}$ abl pre–B cells, as compared with *H2ax*$^{-/-}$*p53*$^{-/-}$ and *Artemis*$^{-/-}$*p53*$^{-/-}$ abl pre–B cells (unpublished data). Although these data are consistent with a role of H2AX in promoting chromatin changes that hold together unrepaired coding ends persisting into S phase, potential effects of mutations in cell cycle checkpoints that arise during v-abl–mediated immortalization more frequently or profoundly in *H2ax*$^{-/-}$ cells than in *H2ax*$^{+/+}$ cells could contribute to this observation.

H2AX prevents chromosome breaks emanating from unrepaired TCR-α/δ locus coding ends

We next sought to test our hypothesis that H2AX prevents unrepaired coding ends from transitioning into chromosome breaks and translocations during continued cell cycle progression using primary lymphocytes. This approach also enables assessment of this potential H2AX function during a physiological cell cycle rather than during recovery from the prolonged G1 arrest associated with STI571 treatment and release. Although a small fraction of unrepaired coding ends persists into S phase in normal primary thymocytes (Pedraza-Alva et al., 2006), we decided to dramatically increase the percentage of cells with unrepaired coding ends for analyses by using *Artemis*$^{-/-}$ thymocytes. Because *Artemis*$^{-/-}$ cells with unrepaired coding ends are eliminated by p53-mediated apoptosis (Rooney et al., 2004), we also needed to use p53 deficiency to allow thymocytes with unrepaired coding ends to survive and proliferate. We first generated germline *H2ax*$^{-/-}$*p53*$^{-/-}$, *Artemis*$^{-/-}$*p53*$^{-/-}$, and *H2ax*$^{-/-}$*Artemis*$^{-/-}$*p53*$^{-/-}$ mice to test our hypothesis. Unfortunately, *H2ax*$^{-/-}$*Artemis*$^{-/-}$*p53*$^{-/-}$ mice rapidly succumbed to multiple malignancies, preventing analysis of unrepaired coding ends in nonmalignant thymocytes. We reasoned that the specific deletion of *H2ax* and/or *p53* in *Artemis*$^{-/-}$ thymocytes should prevent early onset of lymphomas and provide the requisite in vivo experimental system. Transgenic mice expressing Cre under control of the proximal *Lck* promoter (*Lck*-Cre mice) direct excision of target genes such as floxed p53 (*p53*^{F}) in thymocytes before the initiation of V(D)J recombination (Orban et al., 1992; Lee et al., 2001). Thus, we generated *Lck*-Cre*Artemis*$^{-/-}$*p53*$^{F/F}$ (*LAP*), *Lck*-Cre*H2ax*$^{F/F}$*p53*$^{F/F}$ (*LHP*), and *Lck*-Cre*Artemis*$^{-/-}$*H2ax*$^{F/F}$*p53*$^{F/F}$ (*LAHP*) mice. All mice were created heterozygous for *Lck*-Cre to avoid potential complications associated with transgene integration site. The low cellularity of *LAP* and *LAHP* thymocytes posed an insurmountable obstacle for quantitative cytogenetic analyses. Thus, we cultured bone marrow from *LHP*, *LAP*, and *LAHP* mice on OP9-DL1 stromal cells and prepared metaphase spreads from ckit^{-}CD25^{+}CD4^{-}CD8^{-} thymocytes in which normal TCR rearrangements occur (Schmitt and Zúñiga-Pflücker, 2002).

In mouse thymocytes, V(D)J recombination occurs at TCR-α/δ loci on chromosome 14, TCR-β loci on chromosome 6, TCR-γ loci on chromosome 13, and, to a limited extent, Igh loci on chromosome 12. TCR-γ translocations are rarely observed in human and mouse αβ T cells and T lineage lymphomas. Thus, to assay for potential chromosome breaks and translocations initiating from unrepaired RAG-generated coding ends, we hybridized whole chromosome 14, 6, and 12 paints and conducted FISH with BAC probes that hybridize to genomic sequences 5′ or 3′ of TCR-α/δ, TCR-β, or IgH loci on metaphase spreads prepared from *LHP*, *LAP*, and *LAHP* thymocytes (Fig. 5 a). For this purpose, we prepared metaphase spreads from independent thymocyte cultures from two different 3–5-wk-old mice of each genotype. We analyzed 200 or more metaphases for each chromosome paint and FISH probe set on each culture. Chromosome breaks or translocations involving antigen receptor loci were scored when the 5′ and 3′ FISH probe signals were noncoincident (Fig. 5 a). Through this approach, we did not find any chromosome 12 or IgH locus breaks or translocations in metaphases prepared from *LAHP*, *LHP*, or *LAP* thymocytes (Fig. 5 a). However, we observed a modest increase in the frequency of chromosome 6 breaks and translocations involving TCR-β loci in metaphases prepared from *LAHP* thymocytes, as compared with in metaphases prepared from *LHP* or *LAP* thymocytes (Fig. 5, a and b). These findings indicate that structural abnormalities of chromosome 6 and 12 are not frequent occurrences in primary thymocytes deficient in H2AX and/or Artemis but suggest that H2AX may suppress TCR-β translocations. Notably, we observed a substantial increase in the frequency of chromosome 14 abnormalities involving TCR-α/δ loci in metaphases prepared from *LAHP* thymocytes, as compared with those prepared from *LHP* or *LAP* thymocytes (Fig. 5, a and b). All chromosome 14 abnormalities in *LAHP* cells were replicated TCR-α/δ chromosome breaks and, among the metaphases with these lesions, ∼90% contained replicated breaks on a single copy of chromosome 14 (Fig. 5 c). Although we cannot exclude the possibility that these TCR-α/δ chromosome abnormalities represent rare events in a few DN thymocytes that preferentially expand, our data still support a role of H2AX in preventing accumulation of such cells. Based upon these data, we conclude that

H2AX-mediated chromatin changes along RAG-cleaved antigen receptor loci prevent unrepaired coding ends from transitioning into chromosome breaks during continued cell cycle progression.

DISCUSSION

The mechanisms by which H2AX suppresses translocations during V(D)J recombination have remained enigmatic since the findings that a significant percentage of *H2ax*$^{-/-}$ αβ

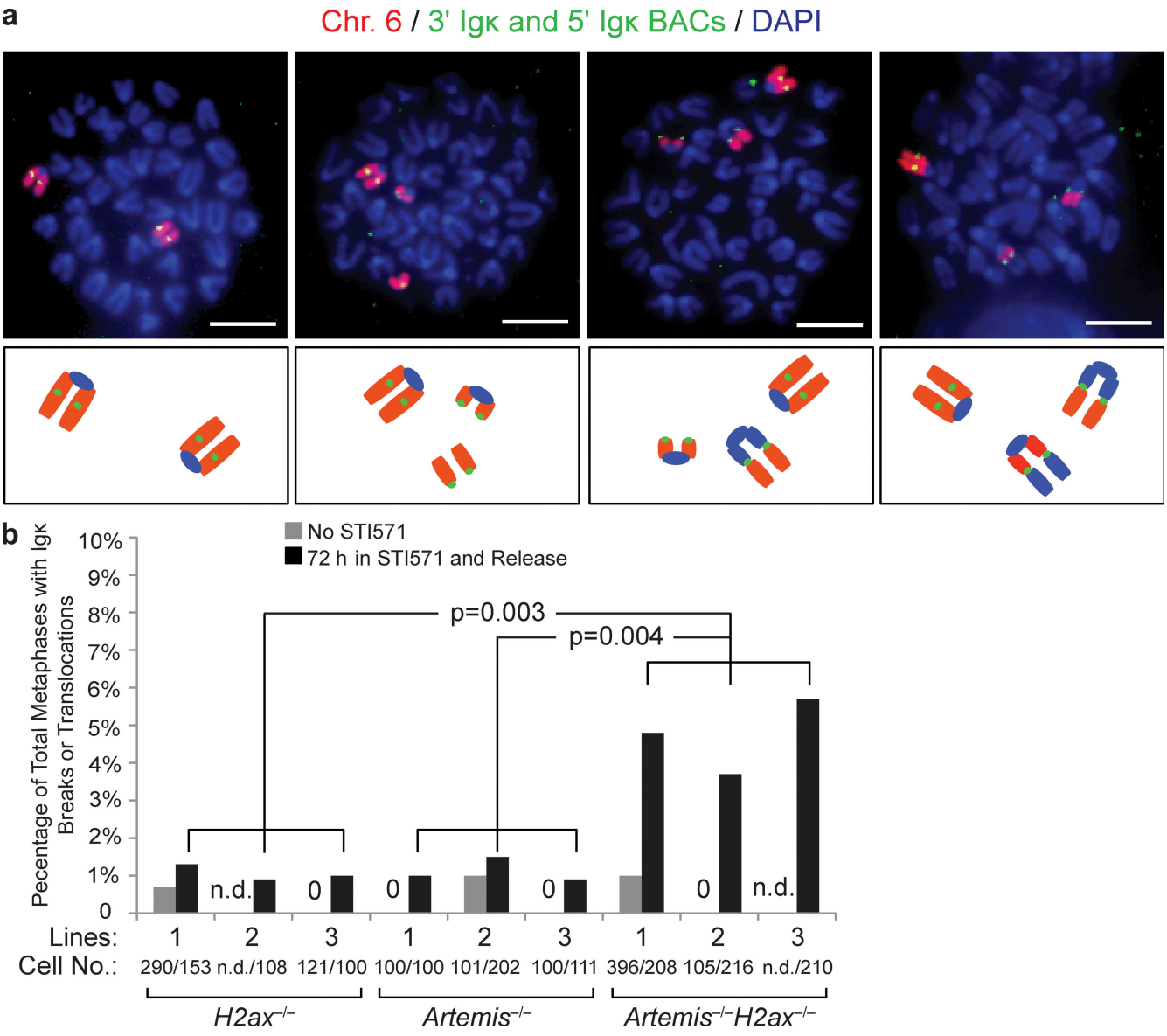

Figure 4. H2AX prevents transition of RAG-cleaved Igκ DNA strands into chromosome breaks and translocations during cellular proliferation. (a) Shown are representative fluorescent light microscopy images of whole chromosome (Chr.) 6 paints (red) and FISH analysis using the 5′ Vκ and 3′ Cκ BACs (both green) and DAPI (blue) to visualize DNA on metaphases prepared from STI571-treated and released *Artemis*$^{-/-}$*H2ax*$^{-/-}$ abl pre–B cells. Below each image is a schematic representation of the observed chromosome 6 configurations. Images show from left to right: two intact chromosome 6; an intact chromosome 6 and a chromosome 6 with an Igκ locus break; an intact chromosome 6 and a chromosome 6 broken into two fragments with one resolved as an Igκ locus translocation; and an intact chromosome 6 and a broken chromosome 6 that resolved as two distinct Igκ locus translocations. Bars, ∼1 µm. (b) Shown is a bar graph with quantification of RAG-initiated Igκ chromosome breaks or translocations in metaphases prepared from cells of three independent *H2ax*$^{-/-}$, *Artemis*$^{-/-}$, and *Artemis*$^{-/-}$*H2ax*$^{-/-}$ pre–B cell lines released from STI571 treatment. Metaphases prepared from cells of the same lines without STI571 treatment were assayed for Igκ chromosome breaks or translocations to control for potential spontaneous rearrangement and genomic instability accumulated during cell culture. The data represents the percentage of total metaphases analyzed that contained Igκ chromosome abnormalities. The numbers of metaphases assayed to generate the representative data are indicated. 0, Igκ abnormalities were not observed; n.d., not determined. The p-values for comparison between cells of the indicated different genotypes are shown. These data were obtained from the same experiment performed three independent times.

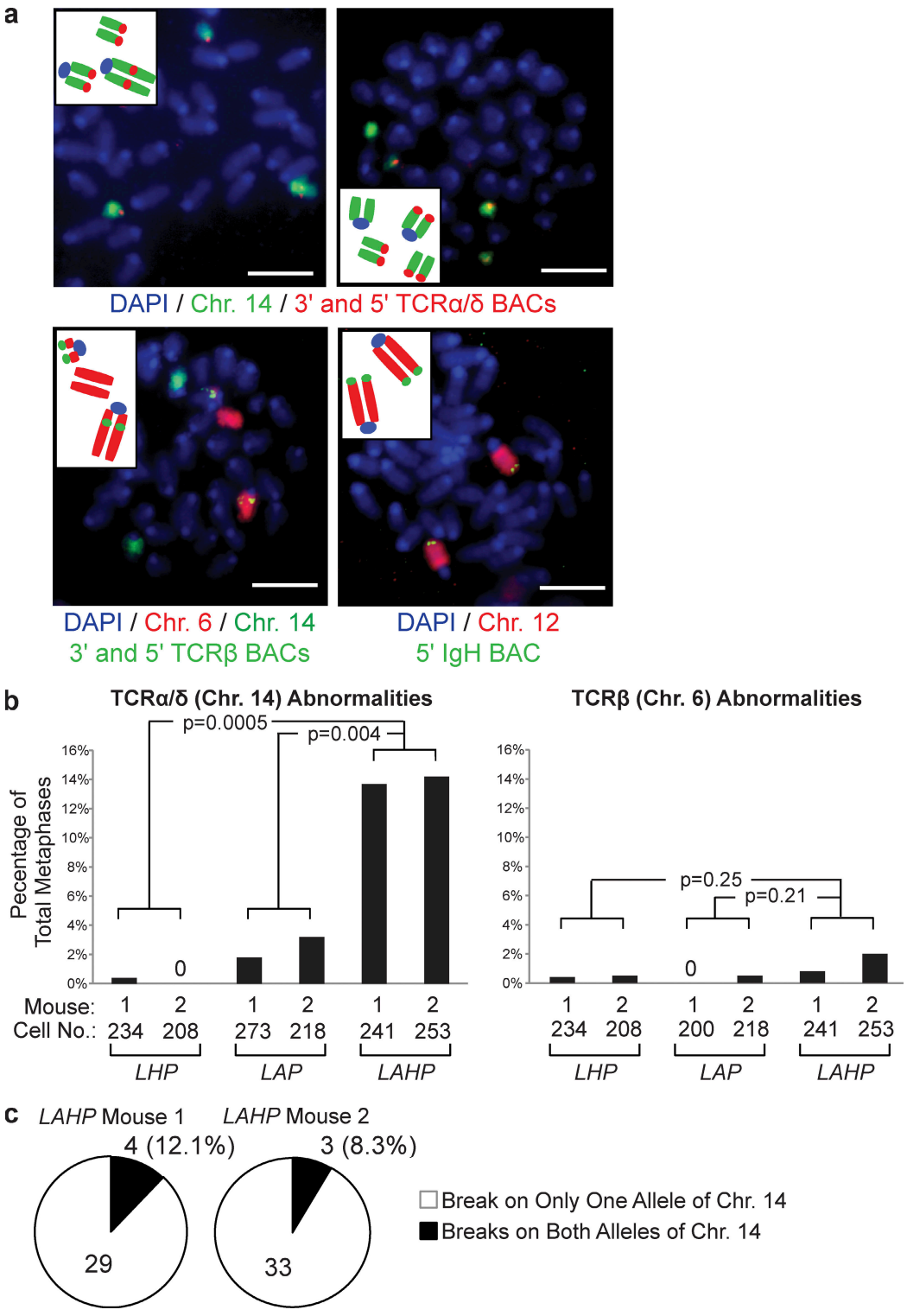

Figure 5. H2AX prevents chromosome breaks emanating from unrepaired TCR-α/δ locus coding ends in primary thymocytes. (a) Shown are representative fluorescent light microscopy images of whole chromosome paints and FISH analysis of antigen receptor loci on metaphases prepared from OP9 primary thymocytes. The insets contain schematics depicting the chromosome abnormalities within each metaphase. Chromosome 14 paints (green) and FISH with 5′ Vα and 3′ Cα BACs (both red) and DAPI (blue) to visualize DNA are shown in the top. Chromosome 6 paint (red) and FISH with 5′ Vβ and 3′ Cβ BACs (both green) and DAPI (blue) to visualize DNA are shown in the bottom left. Chromosome 12 paint (red) and FISH with a 5′ V_H BAC (green) and DAPI (blue) to visualize DNA are shown in the bottom right. Bars, ∼ 2 µm. (b) Shown are bar graphs with quantification of chromosome abnormalities involving TCR-α/δ loci (left) or TCR-β loci (right) in metaphases prepared from primary thymocytes of two independent *LHP*, *LAP*, and *LAHP*

T cells contain TCR-α/δ locus translocations and *H2ax*$^{-/-}$ *p53*$^{-/-}$ mice develop pro–B lymphomas with RAG-initiated IgH/c-myc translocations (Bassing et al., 2003; Celeste et al., 2003). We have demonstrated in this paper that H2AX is not required for the joining of chromosomal coding ends during V(D)J recombination in G1-phase lymphocytes. In this context, we have shown that H2AX deficiency in abl pre–B cells does not lead to accumulation of unrepaired coding ends during the rearrangement of chromosomal substrates, as we previously observed in abl pre–B cells deficient for ATM or DNA-PKcs (Bredemeyer et al., 2006). These data are consistent with the observations that lymphocyte development in *H2ax*$^{-/-}$ mice is not blocked or impaired at stages in which antigen receptor variable region genes are assembled, as is the case in *DNA-PKcs*$^{-/-}$ and *Atm*$^{-/-}$ mice (Bosma et al., 1983; Barlow et al., 1996; Elson et al., 1996; Xu et al., 1996; Gao et al., 1998; Taccioli et al., 1998; Borghesani et al., 2000; Matei et al., 2007; Vacchio et al., 2007). Consequently, we conclude that γ-H2AX formation is not critical for ability of DNA-PKcs and ATM to process and join chromosomal coding ends during variable region gene assembly in G1-phase cells. Although generation of γ-H2AX has been proposed to facilitate DSB repair kinetics by promoting accessibility of broken DNA ends and recruiting repair factors (Rogakou et al., 1998), we did not observe a difference in the kinetics of chromosomal coding join formation between *H2ax*$^{+/+}$ and *H2ax*$^{-/-}$abl pre–B cells. However, potential accessibility and recruitment functions of γ-H2AX might not be evident during V(D)J recombination because initiation of RAG-generated DSBs requires prior opening of chromosomal substrates and the RAG proteins may recruit end-joining factors (Agrawal and Schatz, 1997; Bassing et al., 2002b; Lee et al., 2004; Raval et al., 2008). Thus, we conclude that impaired coding join formation in G1-phase cells is not the predominant mechanism through which translocations arise during V(D)J recombination in H2AX-deficient lymphocytes.

Despite no obvious requirement for H2AX in coding join formation, the data that IgH/c-myc translocations arise by identical mechanisms in *H2ax*$^{-/-}$*p53*$^{-/-}$ mice and NHEJ/p53-deficient mice suggested that H2AX serves critical functions during end joining in G1-phase cells. One advantage of STI571-treated abl pre–B cells is that molecular events associated with V(D)J recombination can be studied in G1-arrested cells. NHEJ-deficient abl pre–B cells offer additional advantages by enabling analysis of particular DSB intermediates and amplification of DNA damage responses. Through the use of *Artemis*$^{-/-}$ and *Artemis*$^{-/-}$*H2ax*$^{-/-}$ abl pre–B cells, we have demonstrated in this paper that H2AX-mediated chromatin changes suppress the physical separation of RAG-cleaved Igκ locus strands in G1-phase cells. This could be caused by the γ-H2AX–mediated anchoring of proteins (such as 53bp1 or cohesins) that hold broken DNA ends together (Bassing and Alt, 2004), modulate flexibility of DNA strands (Difilippantonio et al., 2008; Dimitrova et al., 2008), and/or promote interactions of chromatin with components of the nuclear matrix (Rogakou et al., 1998). Based upon the impaired joining and progression of IgH locus DNA breaks into chromosome breaks and translocations during CSR in *H2ax*$^{-/-}$ B lymphocytes (Reina-San-Martin et al., 2003; Franco et al., 2006; Ramiro et al., 2006), H2AX has been concluded to function in NHEJ by promoting synapsis of DNA ends. Yet, considering that CSR occurs in rapidly proliferating cells (Chaudhuri et al., 2007), these phenotypes could be attributable to H2AX-mediated activation of p53-independent cell cycle checkpoints. Thus, to our knowledge, the data presented in this paper that H2AX suppresses separation of RAG-cleaved DNA strands in G1-arrested cells is the first direct evidence that H2AX exhibits synaptic functions during NHEJ.

Because RAG1/RAG2 can hold CEs and SEs within stable synaptic complexes in vitro (Agrawal and Schatz, 1997; Lee et al. 2004) and ATM maintains chromosomal CEs in proximity (Bredemeyer et al., 2006), our finding that Igκ locus strands with unrepaired CEs separated in *Artemis*$^{-/-}$ cells was unexpected. In this context, ATM alone is not sufficient to prevent disassociation of CEs that are held much less tightly than SEs in the RAG postcleavage complex. However, our observation is in accord with live cell imaging experiments demonstrating mobility of DNA ends at DSBs generated in Ku80-deficient cells (Soutoglou et al., 2007). Our data could reflect baseline mobility of unrepaired Igκ locus DSBs or indicate a role of Artemis in maintaining RAG-generated DNA ends within synaptic complexes, either directly or indirectly through Ku70/Ku80, DNA-PKcs, and/or other end-binding factors. Our finding that H2AX suppresses the physical separation of broken Igκ locus strands appears in contrast with previously published experiments demonstrating a role of Ku80, but not H2AX, in promoting immobility of DSBs (Soutoglou et al., 2007). Upon DSB induction, more unrepaired DNA ends should accumulate in *Ku80*$^{-/-}$ cells as compared with *H2ax*$^{-/-}$ cells as a result of the differential functions of these proteins in end joining. In our study, we used Artemis deficiency to compare the positional stability of disrupted chromosomal DNA strands between *H2ax*$^{+/+}$ and *H2ax*$^{-/-}$ cells that have accumulated equivalent levels of unrepaired DSBs. Thus, we suggest that the disparate conclusions regarding the role of H2AX in maintaining broken chromosomal DNA ends in proximity is the result of a greater level of unrepaired DNA ends that can physically separate in cells deficient for Ku80 versus H2AX.

mice. The numbers of metaphases assayed to generate the data are indicated. Values of 0 mean that no TCR abnormalities were observed. The p-values for comparison between cells of the indicated different genotypes are shown. These data were obtained from the same experiments performed two independent times. (c) Shown are pie charts depicting the percentages of *LAHP* cells with TCR-α/δ chromosome breaks that contain these abnormalities on either one (white) or both (black) allelic copies of chromosome 14.

Although V(D)J recombination occurs in G1-phase cells, some fraction of developing lymphocytes with unrepaired CEs progress into S phase (Rooney et al., 2004). We have shown here that H2AX prevents accumulation of chromosome breaks from RAG-initiated antigen receptor locus DNA breaks that are not repaired before DNA replication. In this context, we have demonstrated that H2AX deficiency in Artemis/p53-deficient thymocytes leads to a substantial increase in the percentage of cells with replicated TCR-α/δ chromosome breaks. Replication through hairpin-sealed CEs should lead to either dicentric or ring chromosomes in metaphase cells. The absence of such chromosome abnormalities in metaphases prepared from *LAP* or *LAHP* thymocytes suggests that TCR-α/δ CEs persisting into S phase are opened before DNA replication. Detection of replicated TCR-α/δ chromosome breaks in *LAHP*, but not *LAP*, metaphases indicates that H2AX holds together DNA strands with unrepaired TCR-α/δ CEs to facilitate end-joining and/or activates the G2/M checkpoint to prevent mitosis. ATM similarly prevents the continued proliferation of lymphocytes with unrepaired RAG-generated coding ends (Callén et al., 2007). Thus, we conclude that ATM-mediated H2AX-dependent chromatin changes along RAG-cleaved antigen receptor loci prevent unrepaired coding ends from transitioning into chromosome breaks during continued cell cycle progression.

The data presented here further contribute to understanding the mechanisms by which chromosomal DSBs are repaired through NHEJ in G1-phase mammalian cells (Fig. 6). Our findings that H2AX, but not ATM or the MRN complex (Bredemeyer et al., 2006; Helmink et al., 2009), is dispensable for end joining of chromosomal CEs in G1 phase cells is consistent with the lower frequency of interlocus V(D)J recombination events and the milder lymphopenia of *H2ax*$^{-/-}$ mice, as compared with *Atm*$^{-/-}$, *Nbs1*$^{m/m}$, and *Mre11*$^{ATLD/ATLD}$ mice (Kang et al., 2002; Theunissen et al., 2003). ATM (Bredemeyer et al., 2006), and likely MRN (Deriano et al., 2009; Helmink et al., 2009), facilitates end joining by maintaining chromosomal CEs within RAG postcleavage synaptic complexes, which engage the proximal ends of cleaved DNA strands. Our observations that γ-H2AX densities are low near Jκ CEs, but elevated over sequences extending at least 500 kb on both sides of Igκ CEs, indicates that γ-H2AX formation stabilizes broken DNA strands at locations distal to breakage sites (Bassing and Alt, 2004). During V(D)J recombination, this ATM-dependent formation of γ-H2AX along RAG-cleaved DNA strands (Savic et al., 2009) is dispensable for end joining of chromosomal CEs in G1 phase cells as a result of cooperation between the DNA end synaptic functions of RAG1/RAG2 and ATM/MRN. In contrast, the ATM-dependent generation of γ-H2AX along DNA strands would

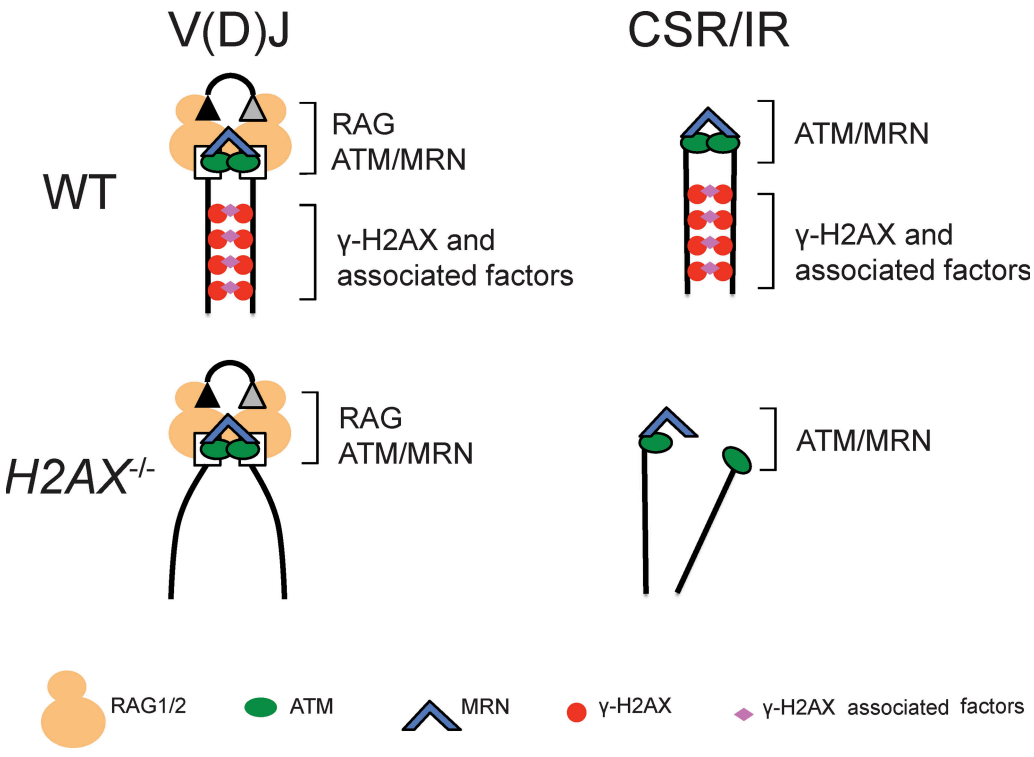

Figure 6. Models of H2AX function during end-joining repair of chromosomal DSBs. Schematic diagrams depicting the potential positional stability of broken chromosomal DNA strands during V(D)J recombination, CSR, or general DSB repair in G1-phase wild-type and H2AX-deficient cells. Boxes and triangle represent RAG-generated coding and signal ends, respectively. H2AX-mediated stabilization of broken DNA strands would be dispensable for end joining during V(D)J recombination as a result of DNA end stabilization by ATM/MRN and RAG postcleavage synaptic complexes. However, this H2AX function would be important for end joining during CSR and general DSB repair.

be more critical for the NHEJ-mediated repair of DSBs generated by genotoxic insults, such as ionizing radiation, or nucleases lacking DNA end synaptic functions, such as those that initiate IgH locus CSR (Fig. 6).

MATERIALS AND METHODS

Mice. All mice were bred and maintained under specific pathogen-free conditions at the Children's Hospital of Philadelphia and were handled according to Institutional Animal Care and Use Committee guidelines. The Institutional Animal Care and Use Committee of the Children's Hospital of Philadelphia approved all of the animal experiments. *H2ax*$^{-/-}$, *H2ax*$^{F/F}$, *Artemis*$^{-/-}$, *p53*$^{F/F}$, *Lck*-Cre transgene, and *Eμ*-Bcl-2 transgene mice have been previously described (Strasser et al., 1991; Jonkers et al., 2001; Lee et al., 2001; Bassing et al., 2002a, 2003; Rooney et al., 2002).

Generation and culture of abl pre–B cell lines. Bone marrow from 3–5-wk-old *H2ax*$^{-/-}$, *H2ax*$^{F/F}$, *H2ax*$^{F/F}$*p53*$^{F/F}$, *Artemis*$^{-/-}$*H2ax*$^{F/F}$, *Artemis*$^{-/-}$*p53*$^{F/F}$, or *Artemis*$^{-/-}$*H2ax*$^{F/F}$*p53*$^{F/F}$ mice harboring the *Eμ*-Bcl-2 transgene were cultured and infected with the pMSCV v-abl retrovirus to generate abl pre–B cell lines of each genotype as previously described (Bredemeyer et al., 2006). Generation of the *Artemis*$^{-/-}$*Rag2*$^{-/-}$ abl pre–B cells was previously described (Savic et al., 2009). *H2ax*$^{-/-}$, *H2ax*$^{F/F}$, *H2ax*$^{F/F}$*p53*$^{F/F}$, and *Artemis*$^{-/-}$*H2ax*$^{F/F}$ abl pre–B cells (10^6/ml) were transduced with pMX-DEL^{CJ} retroviral recombination substrate by cocentrifugation at 1,800 rpm for 90 min. Limiting dilution into 96-well plates and Southern blot analysis was used to isolate clonal cell lines with single pMX-DEJ^{CJ} integrants. Cells were treated with 3 μM STI571 for the indicated times at a density of 10^6 cells/ml. For STI571 release experiments, cells were collected, washed, and then plated into media without STI571 and cultured for ∼10-14 d before metaphase preparation.

Southern blot analysis. Southern blot analyses were performed on genomic DNA using the indicated restriction enzymes and the C4 probe for pMX-DEL^{CJ}, the 3′ Jκ probe for Igκ loci, and a TCR-β VDJ probe for loading control (Bassing et al., 2000; Bredemeyer et al., 2006; Helmink et al., 2009). The extent of Jκ cleavage was calculated by the following formula:

$$\text{Percentage of J}\kappa\text{ cleavage} = \left[1-\frac{\left(\frac{\text{Ig}\kappa\ \text{GL}^{+\text{STI}}}{\text{TCR-}\beta\ \text{GL}^{+\text{STI}}}\right)}{\left(\frac{\text{Ig}\kappa\ \text{GL}^{-\text{STI}}}{\text{TCR-}\beta\ \text{GL}^{-\text{STI}}}\right)}\right]\times 100\%,$$

where the Igκ germline hybridization intensity using the 3′ Jκ probe before or after STI571 treatment (Igκ GL$^{-\text{STI}}$ and Igκ GL$^{+\text{STI}}$, respectively) was normalized to the corresponding TCR-β germline hybridization intensity using the VDJ probe (TCR-β GL$^{-\text{STI}}$ and TCR-β GL$^{+\text{STI}}$, respectively).

ChIP. All data points represent mean values with standard deviation error bars obtained from experiments conducted three times on cells of two independently derived *Artemis*$^{-/-}$ pre–B cell lines. ChIP assays were conducted and data analyzed exactly as described previously (Savic et al., 2009). The sequences of the primers used for quantitative PCR analysis of each genomic location relative to Jκ1 were either described previously (Savic et al., 2009) or are as follows: −250 kb, 5′-CCATCATCAGAACCCAGCATT-3′ and 5′-GCCCTTCTTGACATCCTCTATCA-3′; −650 kb, 5′-AATGGCACAATCCTAGAGGTACAAG-3′ and 5′-CCCTGCTGACTCACTCTCACAT-3′; −1 Mb, 5′-GACCCAAAGAAACAAAACAATAAGG-3′ and 5′-CCCCATCCCCCTCCTAGTT-3′; −1.3 Mb, 5′-AAATGGACATCTTACCGAAAGCA-3′ and 5′-CCTGGGTTTCTTGTTATTCCAAA-3′; and −1.6 Mb, 5′-AGCCAGGTTGGATGTGCTATAAA-3′ and 5′-CACCCAGTCTCCAGCAATCA-3′.

Cytogenetic analyses. Kits for spectral karyotyping and whole chromosome painting were used for metaphase analysis according to the manufacturer's instructions (Applied Spectral Imaging). BAC FISH probes were labeled with Biotin (Biotin-Nick Translation Mix; Roche), and were applied to G1-phase nuclei or metaphase spreads prepared as previously described (Hewitt et al., 2009). The 5′ Vκ (RP24-243E11) and 3′ Cκ (RP23-341D5) BACs used for 2C-FISH analysis were previously described (Hewitt et al., 2009). The TCR-Cβ-164G11, TCR-Vβ17a-23N16, TCR-Cα-232F19, TCR-Vδ3/Vα6-46G9, and 5′ IgH BAC207 BACs used for FISH analysis of translocations in primary thymocytes have been previously described (Liyanage et al., 2000; Franco et al., 2006). All images were captured and analyzed on a spectral karyotyping workstation using Case Data Manager Version 5.5, installed and configured by Applied Spectral Imaging. The 2C-FISH experiments to assay for DSB positional stability were conducted independently on three different lines of *Rag2*$^{-/-}$, *Artemis*$^{-/-}$, and *Artemis*$^{-/-}$*H2ax*$^{-/-}$ abl pre–B cells. To avoid observer bias, these data of these experiments were conducted and obtained blind of the genotypes, with the exception of one *Artemis*$^{-/-}$ line that was not scored blind.

OP9-DL1 co-culture. Bone marrow cells from 4–6-wk-old mice were harvested and red blood cell lysed. Progenitor cells were enriched using MACS purification columns (Miltenyi Biotec) and antibodies specific for mature hematopoietic lineages (CD24, B220, Mac-1, Gr-1, NK1.1, CD11c, and Thy1.2). Approximately 2 million cells were cultured per well using 24-well plates. Cultures were otherwise treated as previously described (Schmitt and Zúñiga-Pflücker, 2002), except for supplementation with 5 ng/ml of mouse IL-7 and human Flt-3L (R&D Systems).

Statistical analysis. All statistical analysis was performed with two-tailed unpaired Student's *t* tests assuming equal variation in Excel (Microsoft). $P < 0.05$ was considered to be statistically significant.

This work was supported by the Cancer Research Institute Pre-doctoral Emphasis Pathway in Tumor Immunology Training Grant awarded to the University of Pennsylvania (B. Yin and V. Savic); National Institutes of Health Grant R01 AI074953 (B.P. Sleckman); and the Department of Pathology and Laboratory Medicine and Center for Childhood Cancer Research of the Children's Hospital of Philadelphia, the Abramson Family Cancer Research Institute of the University of Pennsylvania School of Medicine, a grant from the Pennsylvania Department of Health, the Pew Scholar in the Biomedical Sciences program, and the National Institutes of Health Grant R01 CA 125195 (C.H. Bassing).

The authors have no conflicting financial interests to declare.

Submitted: 7 June 2009
Accepted: 7 October 2009

REFERENCES

Agrawal, A., and D.G. Schatz. 1997. RAG1 and RAG2 form a stable post-cleavage synaptic complex with DNA containing signal ends in V(D)J recombination. *Cell.* 89:43–53. doi:10.1016/S0092-8674(00)80181-6

Barlow, C., S. Hirotsune, R. Paylor, M. Liyanage, M. Eckhaus, F. Collins, Y. Shiloh, J.N. Crawley, T. Ried, D. Tagle, and A. Wynshaw-Boris. 1996. Atm-deficient mice: a paradigm of ataxia telangiectasia. *Cell.* 86:159–171. doi:10.1016/S0092-8674(00)80086-0

Bassing, C.H., and F.W. Alt. 2004. H2AX may function as an anchor to hold broken chromosomal DNA ends in close proximity. *Cell Cycle.* 3:149–153.

Bassing, C.H., F.W. Alt, M.M. Hughes, M. D'Auteuil, T.D. Wehrly, B.B. Woodman, F. Gärtner, J.M. White, L. Davidson, and B.P. Sleckman. 2000. Recombination signal sequences restrict chromosomal V(D)J recombination beyond the 12/23 rule. *Nature.* 405:583–586. doi:10.1038/35014635

Bassing, C.H., K.F. Chua, J. Sekiguchi, H. Suh, S.R. Whitlow, J.C. Fleming, B.C. Monroe, D.N. Ciccone, C. Yan, K. Vlasakova, et al. 2002a. Increased ionizing radiation sensitivity and genomic instability in the absence of histone H2AX. *Proc. Natl. Acad. Sci. USA.* 99:8173–8178. doi:10.1073/pnas.122228699

Bassing, C.H., W. Swat, and F.W. Alt. 2002b. The mechanism and regulation of chromosomal V(D)J recombination. *Cell.* 109:S45–S55. doi:10.1016/S0092-8674(02)00675-X

Bassing, C.H., H. Suh, D.O. Ferguson, K.F. Chua, J. Manis, M. Eckersdorff, M. Gleason, R. Bronson, C. Lee, and F.W. Alt. 2003. Histone H2AX: a dosage-dependent suppressor of oncogenic translocations and tumors. *Cell*. 114:359–370. doi:10.1016/S0092-8674(03)00566-X

Bassing, C.H., S. Ranganath, M. Murphy, V. Savic, M. Gleason, and F.W. Alt. 2008. Aberrant V(D)J recombination is not required for rapid development of H2ax/p53-deficient thymic lymphomas with clonal translocations. *Blood*. 111:2163–2169. doi:10.1182/blood-2007-08-104760

Bewersdorf, J., B.T. Bennett, and K.L. Knight. 2006. H2AX chromatin structures and their response to DNA damage revealed by 4Pi microscopy. *Proc. Natl. Acad. Sci. USA*. 103:18137–18142. doi:10.1073/pnas.0608709103

Bonner, W.M., C.E. Redon, J.S. Dickey, A.J. Nakamura, O.A. Sedelnikova, S. Solier, and Y. Pommier. 2008. GammaH2AX and cancer. *Nat. Rev. Cancer*. 8:957–967. doi:10.1038/nrc2523

Borghesani, P.R., F.W. Alt, A. Bottaro, L. Davidson, S. Aksoy, G.A. Rathbun, T.M. Roberts, W. Swat, R.A. Segal, and Y. Gu. 2000. Abnormal development of Purkinje cells and lymphocytes in Atm mutant mice. *Proc. Natl. Acad. Sci. USA*. 97:3336–3341. doi:10.1073/pnas.050584897

Bosma, G.C., R.P. Custer, and M.J. Bosma. 1983. A severe combined immunodeficiency mutation in the mouse. *Nature*. 301:527–530. doi:10.1038/301527a0

Bredemeyer, A.L., G.G. Sharma, C.Y. Huang, B.A. Helmink, L.M. Walker, K.C. Khor, B. Nuskey, K.E. Sullivan, T.K. Pandita, C.H. Bassing, and B.P. Sleckman. 2006. ATM stabilizes DNA double-strand-break complexes during V(D)J recombination. *Nature*. 442:466–470. doi:10.1038/nature04866

Bredemeyer, A.L., B.A. Helmink, C.L. Innes, B. Calderon, L.M. McGinnis, G.K. Mahowald, E.J. Gapud, L.M. Walker, J.B. Collins, B.K. Weaver, et al. 2008. DNA double-strand breaks activate a multi-functional genetic program in developing lymphocytes. *Nature*. 456:819–823. doi:10.1038/nature07392

Burma, S., B.P. Chen, M. Murphy, A. Kurimasa, and D.J. Chen. 2001. ATM phosphorylates histone H2AX in response to DNA double-strand breaks. *J. Biol. Chem*. 276:42462–42467. doi:10.1074/jbc.C100466200

Callén, E., M. Jankovic, S. Difilippantonio, J.A. Daniel, H.T. Chen, A. Celeste, M. Pellegrini, K. McBride, D. Wangsa, A.L. Bredemeyer, et al. 2007. ATM prevents the persistence and propagation of chromosome breaks in lymphocytes. *Cell*. 130:63–75. doi:10.1016/j.cell.2007.06.016

Celeste, A., S. Petersen, P.J. Romanienko, O. Fernandez-Capetillo, H.T. Chen, O.A. Sedelnikova, B. Reina-San-Martin, V. Coppola, E. Meffre, M.J. Difilippantonio, et al. 2002. Genomic instability in mice lacking histone H2AX. *Science*. 296:922–927. doi:10.1126/science.1069398

Celeste, A., S. Difilippantonio, M.J. Difilippantonio, O. Fernandez-Capetillo, D.R. Pilch, O.A. Sedelnikova, M. Eckhaus, T. Ried, W.M. Bonner, and A. Nussenzweig. 2003. H2AX haploinsufficiency modifies genomic stability and tumor susceptibility. *Cell*. 114:371–383. doi:10.1016/S0092-8674(03)00567-1

Chaudhuri, J., U. Basu, A. Zarrin, C. Yan, S. Franco, T. Perlot, B. Vuong, J. Wang, R.T. Phan, A. Datta, et al. 2007. Evolution of the immunoglobulin heavy chain class switch recombination mechanism. *Adv. Immunol*. 94:157–214. doi:10.1016/S0065-2776(06)94006-1

Chen, H.T., A. Bhandoola, M.J. Difilippantonio, J. Zhu, M.J. Brown, X. Tai, E.P. Rogakou, T.M. Brotz, W.M. Bonner, T. Ried, and A. Nussenzweig. 2000. Response to RAG-mediated VDJ cleavage by NBS1 and gamma-H2AX. *Science*. 290:1962–1965. doi:10.1126/science.290.5498.1962

Deriano, L., T.H. Stracker, A. Baker, J.H. Petrini, and D.B. Roth. 2009. Roles for NBS1 in alternative nonhomologous end-joining of V(D)J recombination intermediates. *Mol. Cell*. 34:13–25. doi:10.1016/j.molcel.2009.03.009

Difilippantonio, S., E. Gapud, N. Wong, C.Y. Huang, G. Mahowald, H.T. Chen, M.J. Kruhlak, E. Callen, F. Livak, M.C. Nussenzweig, et al. 2008. 53BP1 facilitates long-range DNA end-joining during V(D)J recombination. *Nature*. 456:529–533. doi:10.1038/nature07476

Dimitrova, N., Y.C. Chen, D.L. Spector, and T. de Lange. 2008. 53BP1 promotes non-homologous end joining of telomeres by increasing chromatin mobility. *Nature*. 456:524–528. doi:10.1038/nature07433

Downs, J.A., M.C. Nussenzweig, and A. Nussenzweig. 2007. Chromatin dynamics and the preservation of genetic information. *Nature*. 447:951–958. doi:10.1038/nature05980

Elson, A., Y. Wang, C.J. Daugherty, C.C. Morton, F. Zhou, J. Campos-Torres, and P. Leder. 1996. Pleiotropic defects in ataxia-telangiectasia protein-deficient mice. *Proc. Natl. Acad. Sci. USA*. 93:13084–13089. doi:10.1073/pnas.93.23.13084

Fernandez-Capetillo, O., H.T. Chen, A. Celeste, I. Ward, P.J. Romanienko, J.C. Morales, K. Naka, Z. Xia, R.D. Camerini-Otero, N. Motoyama, et al. 2002. DNA damage-induced G2-M checkpoint activation by histone H2AX and 53BP1. *Nat. Cell Biol*. 4:993–997. doi:10.1038/ncb884

Franco, S., M. Gostissa, S. Zha, D.B. Lombard, M.M. Murphy, A.A. Zarrin, C. Yan, S. Tepsuporn, J.C. Morales, M.M. Adams, et al. 2006. H2AX prevents DNA breaks from progressing to chromosome breaks and translocations. *Mol. Cell*. 21:201–214. doi:10.1016/j.molcel.2006.01.005

Fugmann, S.D., A.I. Lee, P.E. Shockett, I.J. Villey, and D.G. Schatz. 2000. The RAG proteins and V(D)J recombination: complexes, ends, and transposition. *Annu. Rev. Immunol*. 18:495–527. doi:10.1146/annurev.immunol.18.1.495

Gao, Y., J. Chaudhuri, C. Zhu, L. Davidson, D.T. Weaver, and F.W. Alt. 1998. A targeted DNA-PKcs-null mutation reveals DNA-PK-independent functions for KU in V(D)J recombination. *Immunity*. 9:367–376. doi:10.1016/S1074-7613(00)80619-6

Gladdy, R.A., M.D. Taylor, C.J. Williams, I. Grandal, J. Karaskova, J.A. Squire, J.T. Rutka, C.J. Guidos, and J.S. Danska. 2003. The RAG-1/2 endonuclease causes genomic instability and controls CNS complications of lymphoblastic leukemia in p53/Prkdc-deficient mice. *Cancer Cell*. 3:37–50. doi:10.1016/S1535-6108(02)00236-2

Helmink, B.A., A.L. Bredemeyer, B.S. Lee, C.Y. Huang, G.G. Sharma, L.M. Walker, J.J. Bednarski, W.L. Lee, T.K. Pandita, C.H. Bassing, and B.P. Sleckman. 2009. MRN complex function in the repair of chromosomal Rag-mediated DNA double-strand breaks. *J. Exp. Med*. 206:669–679. doi:10.1084/jem.20081326

Hewitt, S.L., B. Yin, Y. Ji, J. Chaumeil, K. Marszalek, J. Tenthorey, G. Salvagiotto, N. Steinel, L.B. Ramsey, J. Ghysdael, et al. 2009. RAG-1 and ATM coordinate monoallelic recombination and nuclear positioning of immunoglobulin loci. *Nat. Immunol*. 10:655–664. doi:10.1038/ni.1735

Jonkers, J., R. Meuwissen, H. van der Gulden, H. Peterse, M. van der Valk, and A. Berns. 2001. Synergistic tumor suppressor activity of BRCA2 and p53 in a conditional mouse model for breast cancer. *Nat. Genet*. 29:418–425. doi:10.1038/ng747

Kang, J., R.T. Bronson, and Y. Xu. 2002. Targeted disruption of NBS1 reveals its roles in mouse development and DNA repair. *EMBO J*. 21:1447–1455. doi:10.1093/emboj/21.6.1447

Kinner, A., W. Wu, C. Staudt, and G. Iliakis. 2008. Gamma-H2AX in recognition and signaling of DNA double-strand breaks in the context of chromatin. *Nucleic Acids Res*. 36:5678–5694. doi:10.1093/nar/gkn550

Lee, J., and S. Desiderio. 1999. Cyclin A/CDK2 regulates V(D)J recombination by coordinating RAG-2 accumulation and DNA repair. *Immunity*. 11:771–781. doi:10.1016/S1074-7613(00)80151-X

Lee, P.P., D.R. Fitzpatrick, C. Beard, H.K. Jessup, S. Lehar, K.W. Makar, M. Pérez-Melgosa, M.T. Sweetser, M.S. Schlissel, S. Nguyen, et al. 2001. A critical role for Dnmt1 and DNA methylation in T cell development, function, and survival. *Immunity*. 15:763–774. doi:10.1016/S1074-7613(01)00227-8

Lee, G.S., M.B. Neiditch, S.S. Salus, and D.B. Roth. 2004. RAG proteins shepherd double-strand breaks to a specific pathway, suppressing error-prone repair, but RAG nicking initiates homologous recombination. *Cell*. 117:171–184. doi:10.1016/S0092-8674(04)00301-0

Liyanage, M., Z. Weaver, C. Barlow, A. Coleman, D.G. Pankratz, S. Anderson, A. Wynshaw-Boris, and T. Ried. 2000. Abnormal rearrangement within the alpha/delta T-cell receptor locus in lymphomas from Atm-deficient mice. *Blood*. 96:1940–1946.

Ma, Y., U. Pannicke, K. Schwarz, and M.R. Lieber. 2002. Hairpin opening and overhang processing by an Artemis/DNA-dependent protein kinase complex in nonhomologous end joining and V(D)J recombination. *Cell*. 108:781–794. doi:10.1016/S0092-8674(02)00671-2

Matei, I.R., R.A. Gladdy, L.M.J. Nutter, A. Canty, C.J. Guidos, and J.S. Danska. 2007. ATM deficiency disrupts Tcra locus integrity and the maturation of $CD4^+CD8^+$ thymocytes. *Blood*. 109:1887–1896. doi:10.1182/blood-2006-05-020917

Muljo, S.A., and M.S. Schlissel. 2003. A small molecule Abl kinase inhibitor induces differentiation of Abelson virus-transformed pre-B cell lines. *Nat. Immunol.* 4:31–37. doi:10.1038/ni870

McElhinny, S.A.N., and D.A. Ramsden. 2004. Sibling rivalry: competition between Pol X family members in V(D)J recombination and general double strand break repair. *Immunol. Rev.* 200:156–164. doi:10.1111/j.0105-2896.2004.00160.x

Orban, P.C., D. Chui, and J.D. Marth. 1992. Tissue- and site-specific DNA recombination in transgenic mice. *Proc. Natl. Acad. Sci. USA*. 89:6861–6865. doi:10.1073/pnas.89.15.6861

Paull, T.T., E.P. Rogakou, V. Yamazaki, C.U. Kirchgessner, M. Gellert, and W.M. Bonner. 2000. A critical role for histone H2AX in recruitment of repair factors to nuclear foci after DNA damage. *Curr. Biol.* 10:886–895. doi:10.1016/S0960-9822(00)00610-2

Pedraza-Alva, G., M. Koulnis, C. Charland, T. Thornton, J.L. Clements, M.S. Schlissel, and M. Rincón. 2006. Activation of p38 MAP kinase by DNA double-strand breaks in V(D)J recombination induces a G2/M cell cycle checkpoint. *EMBO J.* 25:763–773. doi:10.1038/sj.emboj.7600972

Perkins, E.J., A. Nair, D.O. Cowley, T. Van Dyke, Y. Chang, and D.A. Ramsden. 2002. Sensing of intermediates in V(D)J recombination by ATM. *Genes Dev.* 16:159–164. doi:10.1101/gad.956902

Petiniot, L.K., Z. Weaver, C. Barlow, R. Shen, M. Eckhaus, S.M. Steinberg, T. Ried, A. Wynshaw-Boris, and R.J. Hodes. 2000. Recombinase-activating gene (RAG) 2-mediated V(D)J recombination is not essential for tumorigenesis in Atm-deficient mice. *Proc. Natl. Acad. Sci. USA*. 97:6664–6669. doi:10.1073/pnas.97.12.6664

Petiniot, L.K., Z. Weaver, M. Vacchio, R. Shen, D. Wangsa, C. Barlow, M. Eckhaus, S.M. Steinberg, A. Wynshaw-Boris, T. Ried, and R.J. Hodes. 2002. RAG-mediated V(D)J recombination is not essential for tumorigenesis in Atm-deficient mice. *Mol. Cell. Biol.* 22:3174–3177. doi:10.1128/MCB.22.9.3174-3177.2002

Ramiro, A.R., M. Jankovic, E. Callen, S. Difilippantonio, H.T. Chen, K.M. McBride, T.R. Eisenreich, J. Chen, R.A. Dickins, S.W. Lowe, et al. 2006. Role of genomic instability and p53 in AID-induced c-myc-Igh translocations. *Nature*. 440:105–109. doi:10.1038/nature04495

Raval, P., A.N. Kriatchko, S. Kumar, and P.C. Swanson. 2008. Evidence for Ku70/Ku80 association with full-length RAG1. *Nucleic Acids Res.* 36:2060–2072. doi:10.1093/nar/gkn049

Reina-San-Martin, B., S. Difilippantonio, L. Hanitsch, R.F. Masilamani, A. Nussenzweig, and M.C. Nussenzweig. 2003. H2AX is required for recombination between immunoglobulin switch regions but not for intra-switch region recombination or somatic hypermutation. *J. Exp. Med.* 197:1767–1778. doi:10.1084/jem.20030569

Rogakou, E.P., D.R. Pilch, A.H. Orr, V.S. Ivanova, and W.M. Bonner. 1998. DNA double-stranded breaks induce histone H2AX phosphorylation on serine 139. *J. Biol. Chem.* 273:5858–5868. doi:10.1074/jbc.273.10.5858

Rogakou, E.P., C. Boon, C. Redon, and W.M. Bonner. 1999. Megabase chromatin domains involved in DNA double-strand breaks in vivo. *J. Cell Biol.* 146:905–916. doi:10.1083/jcb.146.5.905

Rooney, S., J. Sekiguchi, C. Zhu, H.L. Cheng, J. Manis, S. Whitlow, J. DeVido, D. Foy, J. Chaudhuri, D. Lombard, and F.W. Alt. 2002. Leaky Scid phenotype associated with defective V(D)J coding end processing in Artemis-deficient mice. *Mol. Cell.* 10:1379–1390. doi:10.1016/S1097-2765(02)00755-4

Rooney, S., J. Sekiguchi, S. Whitlow, M. Eckersdorff, J.P. Manis, C. Lee, D.O. Ferguson, and F.W. Alt. 2004. Artemis and p53 cooperate to suppress oncogenic N-myc amplification in progenitor B cells. *Proc. Natl. Acad. Sci. USA*. 101:2410–2415. doi:10.1073/pnas.0308757101

Savic, V., B. Yin, N.L. Maas, A.L. Bredemeyer, A.C. Carpenter, B.A. Helmink, K.S. Yang-Iott, B.P. Sleckman, and C.H. Bassing. 2009. Formation of dynamic gamma-H2AX domains along broken DNA strands is distinctly regulated by ATM and MDC1 and dependent upon H2AX densities in chromatin. *Mol. Cell.* 34:298–310. doi:10.1016/j.molcel.2009.04.012

Schmitt, T.M., and J.C. Zúñiga-Pflücker. 2002. Induction of T cell development from hematopoietic progenitor cells by delta-like-1 in vitro. *Immunity*. 17:749–756. doi:10.1016/S1074-7613(02)00474-0

Soutoglou, E., J.F. Dorn, K. Sengupta, M. Jasin, A. Nussenzweig, T. Ried, G. Danuser, and T. Misteli. 2007. Positional stability of single double-strand breaks in mammalian cells. *Nat. Cell Biol.* 9:675–682. doi:10.1038/ncb1591

Stiff, T., M. O'Driscoll, N. Rief, K. Iwabuchi, M. Löbrich, and P.A. Jeggo. 2004. ATM and DNA-PK function redundantly to phosphorylate H2AX after exposure to ionizing radiation. *Cancer Res.* 64:2390–2396. doi:10.1158/0008-5472.CAN-03-3207

Strasser, A., A.W. Harris, and S. Cory. 1991. bcl-2 transgene inhibits T cell death and perturbs thymic self-censorship. *Cell*. 67:889–899. doi:10.1016/0092-8674(91)90362-3

Stucki, M., and S.P. Jackson. 2006. gammaH2AX and MDC1: anchoring the DNA-damage-response machinery to broken chromosomes. *DNA Repair (Amst.)*. 5:534–543. doi:10.1016/j.dnarep.2006.01.012

Taccioli, G.E., A.G. Amatucci, H.J. Beamish, D. Gell, X.H. Xiang, M.I. Torres Arzayus, A. Priestley, S.P. Jackson, A. Marshak Rothstein, P.A. Jeggo, and V.L. Herrera. 1998. Targeted disruption of the catalytic subunit of the DNA-PK gene in mice confers severe combined immunodeficiency and radiosensitivity. *Immunity*. 9:355–366. doi:10.1016/S1074-7613(00)80618-4

Theunissen, J.W., M.I. Kaplan, P.A. Hunt, B.R. Williams, D.O. Ferguson, F.W. Alt, and J.H. Petrini. 2003. Checkpoint failure and chromosomal instability without lymphomagenesis in Mre11(ATLD1/ATLD1) mice. *Mol. Cell.* 12:1511–1523. doi:10.1016/S1097-2765(03)00455-6

Vacchio, M.S., A. Olaru, F. Livak, and R.J. Hodes. 2007. ATM deficiency impairs thymocyte maturation because of defective resolution of T cell receptor alpha locus coding end breaks. *Proc. Natl. Acad. Sci. USA*. 104:6323–6328. doi:10.1073/pnas.0611222104

Vanasse, G.J., J. Halbrook, S. Thomas, A. Burgess, M.F. Hoekstra, C.M. Disteche, and D.M. Willerford. 1999. Genetic pathway to recurrent chromosome translocations in murine lymphoma involves V(D)J recombinase. *J. Clin. Invest.* 103:1669–1675. doi:10.1172/JCI6658

Ward, I.M., and J. Chen. 2001. Histone H2AX is phosphorylated in an ATR-dependent manner in response to replicational stress. *J. Biol. Chem.* 276:47759–47762.

Xie, A., N. Puget, I. Shim, S. Odate, I. Jarzyna, C.H. Bassing, F.W. Alt, and R. Scully. 2004. Control of sister chromatid recombination by histone H2AX. *Mol. Cell.* 16:1017–1025. doi:10.1016/j.molcel.2004.12.007

Xu, Y., T. Ashley, E.E. Brainerd, R.T. Bronson, M.S. Meyn, and D. Baltimore. 1996. Targeted disruption of ATM leads to growth retardation, chromosomal fragmentation during meiosis, immune defects, and thymic lymphoma. *Genes Dev.* 10:2411–2422. doi:10.1101/gad.10.19.2411